Computational Mechanics 19 (1997) 211 – 227 © Springer-Verlag 1997

Large deformation analysis of rubber based on a reproducing kernel particle method

J.-S. Chen, C. Pan, C.-T. Wu

Abstract A nonlinear formulation of the Reproducing Kernel Particle Method (RKPM) is presented for the large deformation analysis of rubber materials which are considered to be hyperelastic and nearly incompressible. In this approach, the global nodal shape functions derived on the basis of RKPM are employed in the Galerkin approximation of the variational equation to formulate the discrete equations of a boundary-value hyperelasticity problem. Existence of a solution in RKPM discretized hyperelasticity problem is discussed. A Lagrange multiplier method and a direct transformation method are presented to impose essential boundary conditions. The characteristics of material and spatial kernel functions are discussed. In the present work, the use of a material kernel function assures reproducing kernel stability under large deformation. Several of numerical examples are presented to study the characteristics of RKPM shape functions and to demonstrate the effectiveness of this method in large deformation analysis. Since the current approach employs C^m global shape functions, the method demonstrates a superior performance to the conventional finite element methods in dealing with large material distortions.

1 Introduction

The analysis of rubber is a challenging task in computational mechanics due to extremely large deformations and the nearly incompressible nature of rubber. Many finite element methods (FEM) have been developed to handle the volumetric locking resulting from the incompressibility constraint. Among them are the mixed formulation [Herrmann (1965); Key (1969); Tong (1969); Liu, Belytschko, and Chen (1988)], selective reduced integration [Malkas and Hughes (1978)], perturbed Lagrange formulation [Bercovier (1978); Chang, Saleeb, and Li (1991); Chen, Han, Wu, and Duan (1995c)], pressure projection method [Chen et al. (1994, 1995a, 1995b)], incompressible plane-strain element [Liu, Ong, and Uras (1985)], and rank-one filtering method [Chen, Pan, and Chang (1995d)] to suppress pressure oscillation. In addition to the difficulties in dealing with rubber incompressibility, the finite element methods frequently break down when applied to engineering elastomers, in which the excessive deformation in rubber components leads to mesh entanglement.

Recently, considerable research in computational mechanics has been devoted to the development of meshless methods. In these methods, the domain of interest is discretized by a scattered set of points. The success of meshless methods is due to the development of new shape functions that allow the interpolation of field variables to be accomplished at a global level and therefore avoid the use of a mesh. These methods are ideal for model refinement, adaptivity, fracture problems, and large deformation problems. Several meshless methods have been developed, including Smooth Particle Hydrodynamics (SPH) [Monaghan (1982, 1988), Libersky et al. (1993)], Diffuse Element Method (DEM) [Nayroles, Touzot, and Villon (1992)], Element Free Galerkin (EFG) [Belytschko et al. (1994a, 1994b, 1994c, 1995), Lu, Belytschko, and Gu (1994)], and Reproducing Kernel Particle Method (RKPM) [Liu et al. (1995a, 1995b, 1995c, 1995d, 1995e, 1996a, 1996b)].

The earliest development in meshless methods was the SPH method. The foundation of the SPH method is the kernel estimate introduced by Monaghan (1982, 1988). In this method, partial differential equations, such as conservation laws, are transformed into integral equations, and the kernel estimate then provides the approximation to estimate field variables at discrete points. Since the functions are evaluated only at points, the use of a mesh is no longer required. The method is quite successful in dealing with astrophysics involving fluid masses moving arbitrarily in an infinite domain. However, when the SPH method is applied to finite domain problems, the method does not perform as accurately as the finite element methods [Johnson, Peterson, and Stryrk (1993)].

The first meshless method developed for structural analysis was due to Nayroles, Touzot, and Villon (1992). They proposed a Diffuse Element Method that employs moving least-squares interpolants in conjunction with the Galerkin method to provide a mesh-free computational formulation. The accuracy of the method was later improved by Belytschko et al. (1994a, 1994b) and was called the Element Free Galerkin (EFG) method. In EFG, the derivatives of interpolants that were omitted in DEM are included and a more accurate numerical integration method is employed to enhance solution accuracy. The

Communicated by W. K. Liu, 4 September 1996

J.-S. Chen, C. Pan, C.-T. Wu
The University of Iowa,
Department of Mechanical Engineering
& Center for Computer-Aided Design
2133 Engineering Building, Iowa City, IA 52242–1527, USA

Correspondence to: J.-S. Chen

The support of this research by Automotive Research Center sponsored by U. S. Army TARDEC to the University of Iowa is greatly acknowledged.

essential boundary conditions are enforced by the use of the Lagrange multiplier method. Lu, Belytschko, and Gu (1994) later introduced a modified variational method to handle essential boundary conditions.

Alternatively, Reproducing Kernel Particle Methods were proposed by Liu et al. (1995a, 1995b) to improve the accuracy of the SPH method for finite domain problems. In this method, the kernel function is modified by introducing a correction function to meet the reproducing conditions. The resulting modified kernel function exactly reproduces polynomials to a specific order and thereby fulfills the completeness requirement. The shape functions developed from this method were later proven to be equivalent to moving least-squares kernel interpolants if linear basis functions were used [Liu, Li, and Belytschko (1995e)]. Liu et al. (1995c, 1995d, 1996b) also introduced wavelets as the kernel functions and successfully applied RKPM to multiple scale analysis.

In this work, we extend RKPM to nonlinear hyperelasticity. A material kernel function is introduced to form displacement shape functions. This development allows the modeling of highly deformed structure without the continuous re-adjustment of dilation parameters to accommodate the changing distance between particles. The material kernel function is particularly useful in a Lagrangian formulation with reference to the original configuration. The method can also be used in a Lagrangian formulation with reference to current configuration by a mapping through the deformation gradient. One of the differences between RKPM and FEM is the treatment of essential boundary conditions. We first discuss a Lagrange multiplier method to handle essential boundary conditions in hyperelasticity. A modified RKPM shape function that possesses Kronecker delta properties is developed by a transformation method to impose essential boundary conditions. The solution existence conditions of RKPM discretization in hyperelasticity problems are discussed following the similar analysis presented by Chen, Han, Wu, and Duan (1995c) for FEM.

In this study, higher-order rubber strain energy density functions are used to better represent the nonlinear behavior of rubber. Several large deformation problems are analyzed to demonstrate the effectiveness of this method and to study the effect of the dilation parameter and particle spacing irregularity on the RKPM solution accuracy.

2 Review of rubber hyperelasticity

The behavior of rubber is classified as hyperelastic in which the strain energy density function can be defined. The choice of reference configuration influences the kinematics, kinetics, constitutive law, and RKPM formulation. In this paper, the original configuration is selected as the reference configuration in the RKPM calculation. The second Piola-Kirchhoff stress and Green-Lagrangian strain are used as the stress and strain measures, respectively.

Consider an elastic body which initially occupies a region Ω_X with boundary Γ_X. The deformation of a material particle $\boldsymbol{X} \in \Omega_X$ at time t is described by $\boldsymbol{x} = \varphi(\boldsymbol{X}, t)$, and the displacement of the particle $\boldsymbol{X}$ is defined by

$$\boldsymbol{u}(\boldsymbol{X}, t) = \boldsymbol{\varphi}(\boldsymbol{X}, t) - \boldsymbol{X} = \boldsymbol{x}(\boldsymbol{X}, t) - \boldsymbol{X} \tag{2.1}$$

where φ is injective in Ω_X and the deformation is orientation-preserving. We consider the reference frame to be a rectangular Cartesian system. The deformation gradient, $\boldsymbol{F}$, Green-Lagrangian strain, $\boldsymbol{E}$, and Green deformation tensor, $\boldsymbol{G}$, are defined by

$$F_{ij} = \frac{\partial x_i}{\partial X_j} = \frac{\partial u_i}{\partial X_j} + \delta_{ij} \tag{2.2}$$

$$E_{ij} = \frac{1}{2}(F_{ki}F_{kj} - \delta_{ij}) \tag{2.3}$$

$$G_{ij} = 2E_{ij} + \delta_{ij} \tag{2.4}$$

The 2nd Piola Kirchhoff stress $\boldsymbol{S}$- the energetically conjugate stress of Green-Lagrangian strain – is defined by

$$S_{ij} = \frac{\partial W}{\partial E_{ij}} \tag{2.5}$$

where W is the strain energy density function which is given for a hyperelastic material. The incremental stress-strain relation is given by

$$\Delta S_{ij} = C_{ijkl}\Delta E_{kl} \tag{2.6}$$

where

$$C_{ijkl} = \frac{\partial^2 W}{\partial E_{ij}\partial E_{kl}} \tag{2.7}$$

and C_{ijkl} is the material response tensor. As discussed by Chang, Saleeb, and Li (1991), and Chen, Wu, and Pan (1995a, 1995b), the strain energy density function for nearly incompressible hyperelastic materials can be written as

$$W(\bar{I}_1, \bar{I}_2, J) = \overline{W}(\bar{I}_1, \bar{I}_2) + \tilde{W}(J) \tag{2.8}$$

$\overline{W}(\bar{I}_1, \bar{I}_2)$ and $\tilde{W}(J)$ are the distortional and dilatational strain energy density functions, respectively, given by

$$\overline{W}(\bar{I}_1, \bar{I}_2) = \sum_{m+n=1}^{\infty} A_{mn}(\bar{I}_1 - 3)^m(\bar{I}_2 - 3)^n \tag{2.9}$$

$$\tilde{W}(J) = \frac{k}{2}(J-1)^2 \tag{2.10}$$

where A_{mn} are material constants, k is the bulk modulus, and $\bar{I}_1$ and $\bar{I}_2$ are the reduced invariants proposed by Penn (1970) to separate the distortional and dilatational deformation:

$$\bar{I}_1 = I_1 I_3^{-1/3} \tag{2.11}$$

$$\bar{I}_2 = I_2 I_3^{-2/3} \tag{2.12}$$

and I_1, I_2, I_3 are the first, second, and third invariants of the Green deformation tensor, respectively, and $J = I_3^{1/2}$. The second Piola-Kirchhoff stress associated with the strain energy density function defined in Eq. (2.8) is

$$S_{ij} = 2[\overline{K}_1 I_3^{-1/3}(\delta_{ij} - \frac{1}{3} I_1 G_{ij}^{-1}) + \overline{K}_2 I_3^{-2/3}(I_1 \delta_{ij} - G_{ij} - \frac{2}{3} I_2 G_{ij}^{-1})] + PJG_{ij}^{-1} \quad (2.13)$$

where

$$\overline{K}_n = \frac{\partial \overline{W}}{\partial \overline{I}_n} \quad , \quad n = 1, 2 \quad (2.14)$$

It can be shown [Chang, Saleeb, and Li (1991)] that the hydrostatic pressure P can be related to $\tilde{W}(J)$ by

$$P = \frac{\partial \tilde{W}}{\partial J} \quad (2.15)$$

Similarly, the material response tensor is obtained according to Eq. (2.7)

$$C_{ijkl} = \overline{C}_{ijkl} + \tilde{C}_{ijkl} \quad (2.16)$$

The explicit expressions of $\overline{C}_{ijkl}$ and $\tilde{C}_{ijkl}$ are given in Appendix A.

3 Reproducing kernel particle method

3.1 Construction of a kernel function

Consider the following kernel estimate of a function $u(x)$

$$u^R(x) = \int_{-\infty}^{\infty} \Phi(x - s) u(s) \mathrm{d}s \quad (3.1)$$

where $u^R(x)$ is the reproduced function and $\Phi(x - s)$ is the kernel function. If the kernel function is a Dirac delta function, then $u^R(x)$ exactly reproduces $u(x)$. In practice, the domain is finite in structural problems. Furthermore, the Dirac delta function is difficult to deal with numerically, and functions such as Gaussian function or spline functions with small supports are usually used. Hence in computation Eq. (3.1) is approximated by

$$u^a(x) = \int_{\Omega_x} \Phi_a(x - s) u(s) \mathrm{d}s \quad (3.2)$$

where

$$\Phi_a(x - s) = \frac{1}{a} \Phi\left(\frac{x - s}{a}\right) \quad (3.3)$$

and a is called the dilation parameter which controls the size of support. We use $u^a(x)$ to denote the reproduced displacement generated by the kernel estimate with a kernel function of support measure a. In SPH applications, Eq. (3.2) is applied to discretized finite domains, and the numerical solutions exhibit amplitude and phase errors in addition to solution deterioration near boundaries. Liu et al. (1995c) explained this phenomenon by the failure to meet the completeness requirement. To address this problem, consider the following Taylor series expansion of $u(s)$:

$$u(s) = \sum_{n=0}^{\infty} \frac{(s - x)^n}{n!} u^{(n)}(x) \quad (3.4)$$

where $u^{(n)} = \mathrm{d}^n u / \mathrm{d}x^n$. Equation (3.2) is rearranged by substituting Eq. (3.4) into Eq. (3.2) to yield

$$u^a(x) = m_0(x) u(x) + \sum_{n=1}^{\infty} \frac{(-1)^n}{n!} m_n(x) u^{(n)}(x) \quad (3.5)$$

where $m_n(x)$ is the moment defined by

$$m_n(x) = \int_{\Omega_x} (x - s)^n \Phi_a(x - s) \mathrm{d}s \quad (3.6)$$

To preserve N-th order completeness in $u^a(x)$, the kernel function has to satisfy the following conditions:

$$m_0 = 1; \quad (3.7)$$

$$m_k = 0 \qquad \text{for} \qquad k = 1, \ldots, N \quad (3.8)$$

Equations (3.7) and (3.8) are called the reproducing conditions (1995d). Not all the kernel functions satisfy these reproducing conditions. For example, the traditional SPH method fails to handle bounded domains due to the failure to meet these reproducing conditions. Liu et al. (1995c) suggested Eq. (3.2) be rewritten as

$$u^a(x) = \int_{\Omega_x} \overline{\Phi}_a(x; x - s) u(s) \mathrm{d}s \quad (3.9)$$

and

$$\overline{\Phi}_a(x; x - s) = \Phi_a(x - s) C(x; x - s) \quad (3.10)$$

where $\overline{\Phi}_a(x; x - s)$ is the modified kernel function, and $C(x; x - s)$ is called the correction function. $C(x; x - s)$ is constructed to avoid the difficulties resulting from finite domain effects and to minimize the amplitude and phase error. The correction function is expressed by an N-th order polynomial of $(x - s)$, i.e.,

$$C(x; x - s) = \sum_{i=0}^{N} b_i(x)(x - s)^i \equiv \boldsymbol{H}^T(x - s)\boldsymbol{b}(x) \quad (3.11)$$

where

$$\boldsymbol{H}^T(x - s) = [1, x - s, (x - s)^2, \ldots, (x - s)^N] \quad (3.12)$$

$$\boldsymbol{b}^T(x) = [b_0(x), b_1(x), \ldots, b_N(x)] \tag{3.13}$$

and $b_i(x)$'s are functions of x which are determined through satisfying the reproducing conditions. By substituting Eqs. (3.10), (3.11) and (3.4) into Eq. (3.9), one can obtain

$$u^a(x) = \overline{m}_0(x)u(x) + \sum_{n=1}^{\infty} \frac{(-1)^n}{n!} \overline{m}_n(x) u^{(n)}(x) \tag{3.14}$$

where

$$\begin{aligned} \overline{m}_n(x) &= \int_{\Omega_x} (x-s)^n C(x; x-s) \Phi_a(x-s) \mathrm{d}s \\ &= \sum_{k=0}^{N} b_k(x) m_{n+k}(x) \end{aligned} \tag{3.15}$$

The reproducing conditions of this modified kernel function are

$$\overline{m}_0(x) = 1 \tag{3.16}$$

and

$$\overline{m}_i(x) = 0 \qquad \text{for} \qquad i = 1, \ldots, N \tag{3.17}$$

Eqs. (3.16) and (3.17) represent the following set of equations

$$\boldsymbol{M}(x)\boldsymbol{b}(x) = \boldsymbol{g} \tag{3.18}$$

where

$$\boldsymbol{M}(x) = \begin{bmatrix} m_0(x) & m_1(x) & \ldots & m_N(x) \\ m_1(x) & m_2(x) & \ldots & m_{N+1}(x) \\ \cdot & \cdot & \cdot & \cdot \\ m_N(x) & m_{N+1}(x) & \ldots & m_{2N}(x) \end{bmatrix} \tag{3.19}$$

and

$$\boldsymbol{g}^T = \boldsymbol{H}^T(0) = [1, 0, \ldots, 0] \tag{3.20}$$

and therefore $\boldsymbol{b}(x)$ can be solved by

$$\boldsymbol{b}(x) = \boldsymbol{M}^{-1}(x)\boldsymbol{g} \tag{3.21}$$

Finally, the modified kernel function $\overline{\Phi}_a(x; x-s)$ is obtained by

$$\begin{aligned} \overline{\Phi}_a(x; x-s) &= \Phi_a(x-s) C(x; x-s) \\ &= \Phi_a(x-s) \boldsymbol{H}^T(x-s) \boldsymbol{M}^{-1}(x) \boldsymbol{H}(0) \end{aligned} \tag{3.22}$$

We remark that if u is an N-th order polynomial, the reproducing equation in Eq. (3.9) with the modified kernel $\overline{\Phi}_a$ constructed to meet reproducing conditions up to the N-th order exactly reproduces u.

The discretized reproducing equation is obtained by performing numerical integration in Eq. (3.9). An example of discretization is to employ the trapezoidal rule to the reproducing equation to yield

$$u^a(x) \cong \sum_{I=1}^{NP} \overline{\Phi}_a(x; x-x_I) u(x_I) \Delta x_I \equiv \sum_{I=1}^{NP} \Psi_I^a(x) d_I \tag{3.23}$$

and

$$\Psi_I^a(x) = \overline{\Phi}_a(x; x-x_I) \Delta x_I \tag{3.24}$$

where NP is the total number of particles, and $\Psi_I^a(x)$'s can be interpreted as the shape functions of $u^a(x)$.

In principle, we choose $\Phi_a(x-x_I)$ to be positive and have a maximum value at $x = x_I$. The function should quickly approach zero as $|x-x_I|$ exceeds a small number so that the shape function $\Psi_I^a(x)$ associated with node I has interaction with only a small group of surrounding nodes to provide computational efficiency. Many kernel functions have been proposed to achieve this behavior; for example, the exponential function proposed by Belytschko et al. (1994a, 1994c) or Gaussian function and cubic spline function used by Liu et al. (1995a, 1995b). In this paper, we employ the cubic spline function as the kernel function:

$$\begin{aligned} &\Phi_a(x-x_I) \\ &= \begin{cases} \frac{2}{3} - 4\left(\frac{x-x_I}{a}\right)^2 + 4\left(\frac{x-x_I}{a}\right)^3 & \text{for } 0 \le \left|\frac{x-x_I}{a}\right| \le \frac{1}{2} \\ \frac{4}{3} - 4\left(\frac{x-x_I}{a}\right) + 4\left(\frac{x-x_I}{a}\right)^2 - \frac{4}{3}\left(\frac{x-x_I}{a}\right)^3 & \text{for } \frac{1}{2} < \left|\frac{x-x_I}{a}\right| \le 1 \\ 0 & \text{otherwise} \end{cases} \end{aligned} \tag{3.25}$$

Several remarks are given below:

1. Since Φ_a is chosen to be a positive function, $\left\{1, x-s, (x-s)^2, \ldots, (x-s)^N\right\}$ are linearly independent with respect to Φ_a, and hence $\boldsymbol{M}$ is non-singular.
2. The smoothness of the shape function $\Psi_I^a(x)$ depends greatly on the smoothness of the kernel function Φ_a, i.e., if $\Phi_a(x-x_I) \in C^m(\Omega_x)$, then $\Psi_I^a(x) \in C^m(\Omega_x)$.
3. The moment matrix $\boldsymbol{M}$ and its derivatives need to be integrated using the same integration rule as that was used in the discretization of the reproducing equation (Eq. (3.23)) to preserve the reproducing conditions in the discrete sense.
4. In the case where the support of $\Phi_a(x-x_I)$ does not intersect with the boundary, i.e., if $[x_I - a, x_I + a] \subset \Omega_x$, then $m_n = \int_{-a}^{a} z^n \Phi_a(z) \mathrm{d}z$, and $\boldsymbol{M}$ degenerates to constant matrix when particles are equally spaced and trapezoidal rule is used for integration. Figure 1 shows that the shape of the modified kernel function $\overline{\Phi}_a(x-x_I)$ (constructed using a set of linear basis functions $\{1, x-x_I\}$) differs from that of the original kernel function $\Phi_a(x-x_I)$ only when $[x_I - a, x_I + a] \not\subset \Omega_x$.
5. The shape function $\Psi_I^a(x)$ does not possess Kronecker delta properties, i.e., $\Psi_I^a(x_J) \neq \delta_{IJ}$.

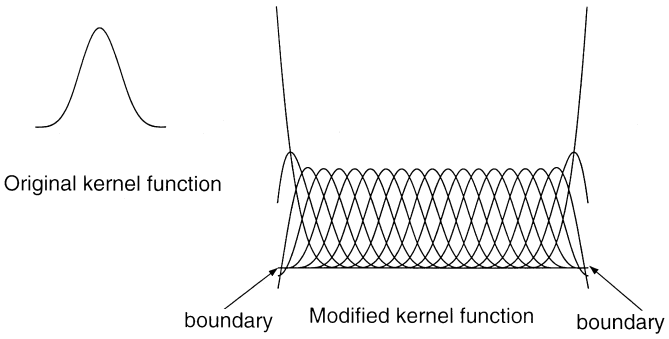

Fig. 1. Kernel Function and modified kernel function

3.2
Multi-dimensional RKPM shape functions

The extension of Φ_a to the multi-dimensional case can be achieved by tensor products of the one-dimensional kernel functions

$$\Phi_a(x - x_I) = \prod_{i=1}^{n_{sd}} \frac{1}{a_i} \Phi\left(\frac{x_i - x_{i_I}}{a_i}\right) \tag{3.26}$$

where n_{sd} is the number of spatial dimensions and a_i is the dilation parameter in the i-th dimension. In this construction, the supports of kernel functions are rectangular and hexahedral in geometries, each with center x_I and dimension $2a_1 \times 2a_2$ and $2a_1 \times 2a_2 \times 2a_3$, in two- and three-dimensional problems, respectively. Alternatively, a multi-dimensional kernel function can be constructed by

$$\Phi\left(\frac{d_I}{a}\right) = \begin{cases} \frac{2}{3} - 4\left(\frac{d_I}{a}\right)^2 + 4\left(\frac{d_I}{a}\right)^3 & \text{for } 0 \le \frac{d_I}{a} \le \frac{1}{2} \\ \frac{4}{3} - 4\left(\frac{d_I}{a}\right) + 4\left(\frac{d_I}{a}\right)^2 - \frac{4}{3}\left(\frac{d_I}{a}\right)^3 & \text{for } \frac{1}{2} \le \frac{d_I}{a} \le 1 \\ 0 & \text{otherwise} \end{cases} \tag{3.27}$$

where

$$d_I = \|\boldsymbol{x} - \boldsymbol{x}_I\| \tag{3.28}$$

Kernel functions defined using Eq. (3.27) have supports of circular and spherical shapes, each with center $\boldsymbol{x}_I$ and radius a, in two- and three-dimensional problems, respectively.

The correction function for the multi-dimensional case is expressed as

$$C(x; x - x_I) = \sum_{|\alpha|=0}^{N} b_{\alpha_1 \alpha_2 \ldots \alpha_{n_{sd}}}(\boldsymbol{x})(x_1 - x_{I_1})^{\alpha_1}(x_2 - x_{I_2})^{\alpha_2} \ldots (x_{n_{sd}} - x_{I_{n_{sd}}})^{\alpha_{n_{sd}}} \tag{3.29}$$

where

$$|\alpha| \equiv \sum_{i=1}^{n_{sd}} \alpha_i \tag{3.30}$$

The coefficients, $b_{\alpha_1 \alpha_2 \ldots \alpha_{n_{sd}}}(x)$'s, are determined from the reproducing conditions. Finally, the multi-dimensional RKPM interpolation is obtained by

$$u_i^a(\boldsymbol{x}) \cong \sum_{I=1}^{NP} \overline{\Phi}_a(\boldsymbol{x}; \boldsymbol{x} - \boldsymbol{x}_I) u_i(\boldsymbol{x}_I) \Delta \mathbf{V}_I \equiv \sum_{I=1}^{NP} \Psi_I^a(\boldsymbol{x}) d_{il} \tag{3.31}$$

where

$$\Psi_I^a(\boldsymbol{x}) = \overline{\Phi}_a(\boldsymbol{x}; \boldsymbol{x} - \boldsymbol{x}_I) \Delta V_I \tag{3.32}$$

and ΔV_I is the volume associated with particle I.

4
RKPM for rubber hyperelasticity

4.1
Variational form and RKPM Galerkin approximation

The simplest and perhaps the most general statement in finite elasticity is to use the first Piola-Kirchhoff stress σ_{ij} and consider the following equilibrium equation

$$\frac{\partial \sigma_{ji}}{\partial X_j} + b_i = 0 \qquad \text{in } \Omega_X \tag{4.1}$$

where $\boldsymbol{b}$ is the body force per unit undeformed volume. The body deformation is subjected to the following natural and essential boundary conditions

$$\sigma_{ji} N_j = h_i \qquad \text{on } \Gamma_X^{h_i} \tag{4.2}$$

$$u_i = g_i \qquad \text{on } \Gamma_X^{g_i} \tag{4.3}$$

where $\boldsymbol{h}$ is the surface force per unit undeformed area on the natural boundary $\Gamma_X^{h_i}$, and $\boldsymbol{g}$ is the prescribed displacement on the essential boundary $\Gamma_X^{g_i}$. For hyperelastic problem, Eqs. (4.1) and (4.2) can be obtained from the stationary conditions of the minimization of the following functional

$$U(\boldsymbol{u}) = \int_{\Omega_X} W(\boldsymbol{u}) \mathrm{d}\Omega - \int_{\Omega_X} u_i b_i \mathrm{d}\Omega - \int_{\Gamma_X^{h_i}} u_i h_i \mathrm{d}\Gamma \tag{4.4}$$

where W is the strain energy density function. In the finite element approach, the essential boundary conditions do not appear in Eq. (4.4) and are imposed by the appropriate selection of test and trial function spaces such that the trial functions satisfy essential boundary conditions and the test functions are homogeneous on the essential boundaries. Because shape functions in finite element methods possess Kronecker delta properties, the aforementioned kinematic constraints can be easily implemented.

In RKPM, on the other hand, shape functions do not possess the Kronecker delta properties. A Lagrange multiplier method is employed to introduce the essential boundary conditions by modifying the functional U to the following form:

$$U(\boldsymbol{u},\boldsymbol{\lambda}) = \int_{\Omega_X} W(\boldsymbol{u})\mathrm{d}\Omega - \int_{\Gamma_X^{h_i}} \lambda_i(u_i - g_i)\mathrm{d}\Omega - \int_{\Omega_X} u_i b_i \mathrm{d}\Omega - \int_{\Gamma_X^{h_i}} u_i h_i \mathrm{d}\Gamma \tag{4.5}$$

where $\boldsymbol{\lambda}$ is the Lagrange multiplier. Note that the minimization problem of Eq. (4.4) subjected to constraint conditions (4.3) is equivalent to a saddle point problem of Eq. (4.5). Taking the variation of Eq. (4.5) leads to

$$\delta U(\boldsymbol{u},\boldsymbol{\lambda}) = \int_{\Omega_X} \delta E_{ij} S_{ij}\mathrm{d}\Omega - \int_{\Gamma_X^{g_i}} \delta\lambda_i(u_i - g_i)\mathrm{d}\Gamma - \int_{\Gamma_X^{g_i}} \delta u_i \lambda_i \mathrm{d}\Gamma - \int_{\Omega_X} \delta u_i b_i \mathrm{d}\Omega - \int_{\Gamma_X^{h_i}} \delta u_i h_i \mathrm{d}\Gamma \tag{4.6}$$

For arbitrary $\delta u_i \neq 0$ and $\delta\lambda_i \neq 0$, the stationary conditions are

$$\int_{\Omega_X} \delta E_{ij} S_{ij}\mathrm{d}\Omega - \int_{\Gamma_X^{g_i}} \delta u_i \lambda_i \mathrm{d}\Gamma - \int_{\Omega_X} \delta u_i b_i \mathrm{d}\Omega - \int_{\Gamma_X^{h_i}} \delta u_i h_i \mathrm{d}\Gamma = 0 \tag{4.7}$$

and

$$\int_{\Gamma_X^{g_i}} \delta\lambda_i(u_i - g_i)\mathrm{d}\Gamma = 0 \tag{4.8}$$

Note that $\int_{\Omega_X} \delta E_{ij} S_{ij}\mathrm{d}\Omega = \int_{\Omega_X} \delta F_{ij}\sigma_{ij}\mathrm{d}\Omega$. We shall now consider incremental small deformations superimposed on a finitely deformed configuration. Let n and ν denote the load step counter and iteration counter, respectively. Suppose the body force, the surface traction, and prescribed displacements at $(n+1)$-th load step are given, and the deformation state of the body at $(n+1)$-th load step and ν-th iteration is known. We are seeking the increments $\Delta\boldsymbol{u} \in H^1$ and $\Delta\boldsymbol{\lambda} \in H^0$, defined by $\boldsymbol{x}_{n+1}^{\nu+1} = \boldsymbol{x}_{n+1}^{\nu} + \Delta\boldsymbol{u}$ and $\boldsymbol{\lambda}_{n+1}^{\nu+1} = \boldsymbol{\lambda}_{n+1}^{\nu} + \Delta\boldsymbol{\lambda}$, such that for all $\delta\boldsymbol{u} \in H^1$ and $\delta\boldsymbol{\lambda} \in H^0$ the following incremental equations are satisfied,

$$\begin{aligned}
&\int_{\Omega_X} \left[\frac{1}{2}\left(F_{pi}\frac{\partial\delta u_p}{\partial X_j} + F_{pj}\frac{\partial\delta u_p}{\partial X_i}\right)_{n+1}^{\nu}\right](C_{ijkl})_{n+1}^{\nu} \\
&\quad\times\left[\frac{1}{2}\left(F_{qk}\frac{\partial\Delta u_q}{\partial X_l} + F_{ql}\frac{\partial\Delta u_q}{\partial X_k}\right)_{n+1}^{\nu}\right]\mathrm{d}\Omega \\
&\quad+\int_{\Omega_X}\frac{\partial\delta u_i}{\partial X_j}(T_{ijkl})_{n+1}^{\nu}\frac{\partial\Delta u_k}{\partial X_l}\mathrm{d}\Omega - \int_{\Gamma_X^{g_i}}\delta u_i\Delta\lambda_i\mathrm{d}\Gamma \\
&\quad= \int_{\Omega_X}\delta u_i(b_i)_{n+1}\mathrm{d}\Omega + \int_{\Gamma_X^{h_i}}\delta u_i(h_i)_{n+1}\mathrm{d}\Gamma \\
&\quad\quad- \int_{\Omega_X}(\delta E_{ij}S_{ij})_{n+1}^{\nu}\mathrm{d}\Omega + \int_{\Gamma_X^{h_i}}\delta u_i(\lambda_i)_{n+1}^{\nu}\mathrm{d}\Gamma
\end{aligned} \tag{4.9}$$

$$\int_{\Gamma_X^{gi}} \delta\lambda_i \Delta u_i \mathrm{d}\Gamma = \int_{\Gamma_X^{gi}} \delta\lambda_i(g_i - u_i)_{n+1}^{\nu}\mathrm{d}\Gamma \tag{4.10}$$

where $T_{ijkl} = \delta_{ik}S_{jl}$ is the initial stress tensor and H^1 and H^0 denote Sobolev spaces with degree one and zero, respectively. To construct discrete RKPM equations, the discrete displacements are formulated by $\Delta u_i^a = \sum_{I=1}^{NP}\Psi_I^a\Delta\mathrm{d}_{il}$ and $\delta u_i^a = \sum_{I=1}^{NP}\Psi_I^a\delta\mathrm{d}_{il}$ where the subscript "a" refers to the RKPM discretization measured by the dilation parameter a. As discussed by Belytschko, Lu, and Gu (1994a), a simple linear Lagrange interpolation function $\Theta_1(c)$, where c is the curvilinear coordinate along the boundary, can be used to interpolate $\Delta\lambda_i^a = \sum_{I=1}^{NB}\Theta_I\Delta\lambda_{il}$ and $\delta\lambda_i^a = \sum_{I=1}^{NB}\Theta_I\delta\boldsymbol{\lambda}_{il}$ on the essential boundaries discretized by NB points. The final RKPM discrete incremental equations are

$$\begin{bmatrix}\boldsymbol{K} & \boldsymbol{G}\\ \boldsymbol{G}^T & \boldsymbol{0}\end{bmatrix}_{n+1}^{\nu}\begin{bmatrix}\Delta\boldsymbol{d}\\ \Delta\boldsymbol{\lambda}\end{bmatrix} = \begin{bmatrix}\Delta\boldsymbol{f}\\ \Delta\boldsymbol{q}\end{bmatrix}_{n+1}^{\nu} \tag{4.11}$$

where

$$\boldsymbol{K} = \boldsymbol{K}^M + \boldsymbol{K}^G \tag{4.12}$$

$$\Delta\boldsymbol{f} = \boldsymbol{f}^{ext} - \boldsymbol{f}^{int} \tag{4.13}$$

$$\boldsymbol{K}_{IJ}^G = \int_{\Omega_X}\boldsymbol{B}_I^{G^T}\boldsymbol{T}\boldsymbol{B}_J^G\mathrm{d}\Omega \tag{4.14}$$

$$\boldsymbol{K}_{IJ}^M = \int_{\Omega_X}\boldsymbol{B}_I^{M^T}\boldsymbol{C}\boldsymbol{B}_J^M\mathrm{d}\Omega \tag{4.15}$$

$$\boldsymbol{G}_{IJ} = -\int_{\Omega_X}\Psi_I^a\Theta_J\boldsymbol{I}\mathrm{d}\Omega \tag{4.16}$$

$$\boldsymbol{f}_I^{ext} = \int_{\Omega_X}\Psi_I^a\boldsymbol{b}\mathrm{d}\Omega + \int_{\Gamma_X^{h_i}}\Psi_I^a\boldsymbol{h}\mathrm{d}\Gamma + \int_{\Gamma_X^{g_i}}\Psi_I^a\boldsymbol{\lambda}^a\mathrm{d}\Gamma \tag{4.17}$$

$$\boldsymbol{f}_I^{int} = \int_{\Omega_X}\boldsymbol{B}_I^{G^T}\boldsymbol{\Xi}\mathrm{d}\Omega \tag{4.18}$$

$$\Delta\boldsymbol{q}_I = \int_{\Gamma_X^{gi}}\Theta_I\boldsymbol{V}(\boldsymbol{u} - \boldsymbol{g})\mathrm{d}\Gamma \tag{4.19}$$

For two-dimensional problems,

$$\boldsymbol{B}_I^G = \begin{bmatrix}\frac{\partial\Psi_I^a}{\partial X_1} & 0\\ 0 & \frac{\partial\Psi_I^a}{\partial X_2}\\ \frac{\Psi_I^a}{\partial X_2} & 0\\ 0 & \frac{\partial\Psi_I^a}{\partial X_1}\\ \epsilon\frac{\Psi_I^a}{X_1} & 0\end{bmatrix} \tag{4.20}$$

$$\boldsymbol{B}_I^M = \begin{bmatrix} F_{11}\frac{\partial \Psi_I^a}{\partial X_1} & F_{21}\frac{\partial \Psi_I^a}{\partial X_1} \\ F_{12}\frac{\partial \Psi_I^a}{\partial X_2} & F_{22}\frac{\partial \Psi_I^a}{\partial X_2} \\ F_{11}\frac{\partial \Psi_I^a}{\partial X_2} + F_{12}\frac{\partial \Psi_I^a}{\partial X_1} & F_{21}\frac{\partial \Psi_I^a}{\partial X_2} + F_{22}\frac{\partial \Psi_I^a}{\partial X_1} \\ \epsilon F_{33}\frac{\Psi_I^a}{X_1} & 0 \end{bmatrix} \tag{4.21}$$

$$\boldsymbol{C} = \begin{bmatrix} C_{1111} & C_{1122} & C_{1112} & C_{1133} \\ & C_{2222} & C_{2212} & C_{2233} \\ & & C_{1212} & C_{1233} \\ \text{sym} & & & C_{3333} \end{bmatrix} \tag{4.22}$$

$$\boldsymbol{T} = \begin{bmatrix} S_{11} & 0 & S_{12} & 0 & 0 \\ 0 & S_{22} & 0 & S_{21} & 0 \\ S_{21} & 0 & S_{22} & 0 & 0 \\ 0 & S_{12} & 0 & S_{11} & 0 \\ 0 & 0 & 0 & 0 & S_{33} \end{bmatrix} \tag{4.23}$$

$$\boldsymbol{I} = \begin{bmatrix} 1 & 0 \\ 0 & 1 \end{bmatrix} \tag{4.24}$$

$$\boldsymbol{V} = \begin{bmatrix} \nu_{11} & 0 \\ 0 & \nu_{22} \end{bmatrix};$$

$$\nu_{ii} = \begin{cases} 1 & \text{if displacement in i-th direction is prescribed} \\ 0 & \text{otherwise} \end{cases} \tag{4.25}$$

$$\boldsymbol{\Xi} = \begin{bmatrix} S_{11} \\ S_{22} \\ S_{12} \\ S_{33} \end{bmatrix} \tag{4.26}$$

$$\epsilon = \begin{cases} 1 & \text{for axisymmetric} \\ 0 & \text{for plane strain} \end{cases} \tag{4.27}$$

The Lagrange multiplier method has several drawbacks:

1. The coefficient matrix in Eq. (4.11) is not positive definite, and also not banded.
2. A different set of interpolation functions are needed for displacement defined in the domain and for Lagrange multipliers defined on the boundaries.
3. The Lagrange multipliers defined on the essential boundaries need to be solved in addition to the displacements at each incremental step in nonlinear computation.

To alleviate these difficulties, a direct transformation method is introduced in the next section.

4.2 A direct transformation method

The need to employ the Lagrange multiplier method in the RKPM formulation discussed in the previous section is because the RKPM shape function does not pass through data. With this knowledge, we shall develop a modified RKPM shape function that possesses Kronecker delta properties.

Recall the RKPM shape functions for $\boldsymbol{u}^a$:

$$u_i^a(X) = \sum_{I=1}^{NP} \Psi_I^a(\boldsymbol{X}) d_{iI} \tag{4.28}$$

Letting $\hat{d}_{ij} \equiv u_i^a(\boldsymbol{X}_J)$, we have the following conditions:

$$\hat{d}_{ij} = \sum_{I=1}^{NP} \Psi_I^a(\boldsymbol{X}_J) d_{iI} = \sum_{I=1}^{NP} A_{IJ} d_{iI} \tag{4.29}$$

or

$$d_{iI} = \sum_{K=1}^{NP} A_{KI}^{-1} \hat{d}_{iK} \tag{4.30}$$

where

$$A_{IJ} = \Psi_I^a(\boldsymbol{X}_J) \tag{4.31}$$

By substituting Eq. (4.30) into Eq. (4.28), one can obtain

$$\begin{aligned} u_i^a(\boldsymbol{X}) &= \sum_{I=1}^{NP} \Psi_I^a(\boldsymbol{X}) d_{iI} = \sum_{I=1}^{NP}\sum_{K=1}^{NP} \Psi_I^a(\boldsymbol{X}) A_{KI}^{-1} \hat{d}_{iK} \\ &\equiv \sum_{K=1}^{NP} \hat{\Psi}_K^a(\boldsymbol{X}) \hat{d}_{iK} \end{aligned} \tag{4.32}$$

where

$$\hat{\Psi}_K^a(\boldsymbol{X}) = \sum_{I=1}^{NP} A_{KI}^{-1} \Psi_I^a(\boldsymbol{X}) \tag{4.33}$$

Note that $\hat{\Psi}_I^a(\boldsymbol{X}_J) = \sum_{K=1}^{NP} A_{IK}^{-1} \Psi_K^a(\boldsymbol{X}_J) = \sum_{K=1}^{NP} A_{IK}^{-1} A_{KJ} = \delta_{IJ}$, and $\hat{d}_{iI} = u_i^a(\boldsymbol{X}_I)$ is the nodal value of u_i^a.

We shall now deal with a minimization problem using the functional given in Eq. (4.4). The corresponding variational statement is:

Given $W, \boldsymbol{b}, \boldsymbol{h}, \boldsymbol{g}$, find $\boldsymbol{u} \in H_g^1$ ($H_g^1 = \{\boldsymbol{v} : \boldsymbol{v} \in H^1, v_i = g_i$ on $\Gamma_x^{g_i}\}$), such that for all $\delta\boldsymbol{u} \in H_0^1$, ($H_0^1 = \{\boldsymbol{v} : \boldsymbol{v} \in H^1$, $v_i = 0$ on $\Gamma_x^{g_i}\}$), the following equation is satisfied:

$$\begin{aligned} \delta U(\boldsymbol{u}) = &\int_{\Omega_x} \delta E_{ij}(\boldsymbol{u}) S_{ij}(\boldsymbol{u}) \mathrm{d}\Omega \\ &- \int_{\Omega_x} \delta u_i b_i \mathrm{d}\Omega - \int_{\Gamma_x^{h_i}} \delta u_i h_i \mathrm{d}\Gamma = 0 \end{aligned} \tag{4.34}$$

Let $\delta\boldsymbol{u}^a$ and $\boldsymbol{u}^a$ be the RKPM approximation of $\delta\boldsymbol{u}$ and $\boldsymbol{u}$, respectively. The problem statement of the Galerkin approximation is:

Given $W, \boldsymbol{b}, \boldsymbol{h}, \boldsymbol{g}$, find $\boldsymbol{u}^a \in H_g^1$, such that for all $\delta\boldsymbol{u}^a \in H_0^1$, the following equation is satisfied

$$\begin{aligned} \delta U(\boldsymbol{u}^a) = &\int_{\Omega_x} \delta E_{ij}(\delta\boldsymbol{u}^a) S_{ij}(\boldsymbol{u}^a) \mathrm{d}\Omega \\ &- \int_{\Omega_x} \delta u_i^a b_i \mathrm{d}\Omega - \int_{\Gamma_x^{h_i}} \delta u_i^a h_i \mathrm{d}\Gamma = 0 \end{aligned} \tag{4.35}$$

Note that $\boldsymbol{u}^a$ and $\delta\boldsymbol{u}^a$ satisfy the following boundary conditions,

$$u_i^a(\boldsymbol{X}_I) = \sum_{J=1}^{NP} \hat{\Psi}_J^a(\boldsymbol{X}_I)\hat{\mathrm{d}}_{iJ} = g_i(\boldsymbol{X}_I) \qquad \forall I \in \eta_{gi} \tag{4.36}$$

$$\delta u_i^a(\boldsymbol{X}_I) = \sum_{J=1}^{NP} \hat{\Psi}_J^a(\boldsymbol{X}_I)\delta\hat{\mathrm{d}}_{iJ} = 0 \qquad \forall I \in \eta_{gi} \tag{4.37}$$

where η_{gi} denote a set of particle numbers in which the associated particles are located on Γ_X^{gi}. Since $\hat{\Psi}_I^a(\boldsymbol{X}_J) = \delta_{IJ}$, the unknown coefficients can be directly obtained:

$$\hat{\mathrm{d}}_{iI} = g_i(\boldsymbol{X}_I) \qquad \forall I \in \eta_{gi} \tag{4.38}$$

$$\delta\hat{\mathrm{d}}_{iI} = 0 \qquad \forall I \in \eta_{gi} \tag{4.39}$$

The equation described in Eq. (4.35) is solved incrementally and the problem statement for the incremental equation is:
Given $\boldsymbol{b}_{n+1}, \boldsymbol{h}_{n+1}, \Delta\boldsymbol{g}_{n+1}, \boldsymbol{x}_{n+1}^{\nu}, \boldsymbol{F}_{n+1}^{\nu}, \boldsymbol{S}_{n+1}^{\nu}$, find $\Delta\boldsymbol{u}^a \in H_{\Delta g}^1$, such that for all $\delta\boldsymbol{u}^a \in H_0^1$, the following incremental equation is satisfied:

$$\begin{aligned}
&\int_{\Omega_X} \left[\frac{1}{2}\left(F_{pi}\frac{\partial\delta u_p^a}{\partial X_j} + F_{pj}\frac{\partial\delta u_p^a}{\partial X_i}\right)^{\nu}_{n+1}\right](C_{ijkl})^{\nu}_{n+1} \\
&\quad\times\left[\frac{1}{2}\left(F_{qk}\frac{\partial\Delta u_q^a}{\partial X_l} + F_{ql}\frac{\partial\Delta u_q^a}{\partial X_k}\right)^{\nu}_{n+1}\right]\mathrm{d}\Omega \\
&\quad+\int_{\Omega_X}\frac{\partial\delta u_i^a}{\partial X_j}(\boldsymbol{T}_{ijkl})^{\nu}_{n+1}\frac{\partial\Delta u_k^a}{\partial X_l}\mathrm{d}\Omega \\
&=\int_{\Omega_X}\delta u_i^a(b_i)_{n+1}\mathrm{d}\Omega + \int_{\Gamma_X^{h_i}}\delta u_i^a(h_i)_{n+1}\mathrm{d}\Gamma \\
&\quad-\int_{\Omega_X}(\delta E_{ij}S_{ij})^{\nu}_{n+1}\mathrm{d}\Omega
\end{aligned} \tag{4.40}$$

By substituting Eq. (4.28) into Eq. (4.35), in conjunction with the tangent operator in Eq. (4.40), the following discretized RKPM incremental equilibrium equation is obtained:

$$\hat{\boldsymbol{K}}\Delta\hat{\boldsymbol{d}} = \Delta\hat{\boldsymbol{f}} \tag{4.41}$$

where

$$\hat{\boldsymbol{K}} = \boldsymbol{\Lambda}^{-1}\boldsymbol{K}\boldsymbol{\Lambda}^{-T} \tag{4.42}$$

$$\Delta\hat{\boldsymbol{f}} = \boldsymbol{\Lambda}^{-1}(\boldsymbol{f}^{ext} - \boldsymbol{f}^{int}) \tag{4.43}$$

$$\Delta\hat{\boldsymbol{d}} = \boldsymbol{\Lambda}^{-T}\Delta\boldsymbol{d} \tag{4.44}$$

$$\boldsymbol{\Lambda}_{ij} = A_{ij}I \tag{4.45}$$

and $\boldsymbol{I}$ is the identity matrix. Note that $\boldsymbol{\Lambda}^{-1}\boldsymbol{f}^{ext}$ and $\boldsymbol{\Lambda}^{-1}\boldsymbol{f}^{int}$ are the nodal external force and internal force vectors, respectively. Consequently, the point load can be directly applied.

4.3 Material and spatial kernel functions

4.3.1 Material kernel function

In Lagrangian computation, the RKPM particles coincide with material particles throughout deformation. In the present work, a Lagrangian formulation is used in hyperelasticity and all the kinematic and kinetic variables are referenced to the original configuration. Therefore, the RKPM shape function, and more precisely, the kernel function, is to be constructed in the original configuration. One can express the kernel function in the original configuration, referred to as material kernel function, in the following form:

$$\Phi_a^X(\boldsymbol{X} - \boldsymbol{X}_I) = \frac{1}{a}\Phi\left(\frac{\|\boldsymbol{X} - \boldsymbol{X}_I\|}{a}\right) \tag{4.46}$$

This material kernel function $\Phi_a^X(\boldsymbol{X} - \boldsymbol{X}_1)$ has fixed support size in the original configuration and has a deformation dependent support size when mapped to the current configuration. The support of the function covers the same set of material particles with a fixed dilation parameter a when the structure deforms. This material kernel function fits naturally into the Lagrangian formulation, since in this paper the Lagrangian RKPM matrices are integrated over the original configuration.

When the Lagrangian formulation is referenced to the current configuration, the material kernel function is constructed by mapping the current position vector $\boldsymbol{x}$ to $\boldsymbol{X} = \boldsymbol{\varphi}^{-1}(\boldsymbol{x}, t)$ to yield

$$\begin{aligned}
&\Phi_a^X(\boldsymbol{\varphi}^{-1}(\boldsymbol{x}, t) - \boldsymbol{\varphi}^{-1}(\boldsymbol{x}_I, t)) \\
&\qquad = \frac{1}{a}\Phi\left(\frac{\|\boldsymbol{\varphi}^{-1}(\boldsymbol{x}, t) - \boldsymbol{\varphi}^{-1}(\boldsymbol{x}_I, t)\|}{a}\right)
\end{aligned} \tag{4.47}$$

We remark that when the material kernel function is employed in the Lagrangian formulation with reference to the current configuration, the spatial derivatives of the material kernel function are obtained by the following chain rule:

$$\frac{\partial\Phi_a^X(\boldsymbol{X} - \boldsymbol{X}_I)}{\partial x_i} = \frac{\partial\Phi_a^X(\boldsymbol{X} - \boldsymbol{X}_I)}{\partial X_j}F_{ji}^{-1}\Big|_{\substack{\boldsymbol{X}=\varphi^{-1}(x,t)\\ \boldsymbol{X}_I=\varphi^{-1}(x_I,t)}} \tag{4.48}$$

The characteristics of the material kernel function are illustrated in the following one-dimensional uniaxial tension problem,

$$x = \varphi(X, t) = (1 + t)X \tag{4.49}$$

or

$$X = \varphi^{-1}(x, t) = \frac{x}{(1 + t)} \tag{4.50}$$

The material kernel function expressed in the material coordinate is

$$\Phi_a^X(X - X_I) = \frac{1}{a}\Phi\left(\frac{|X - X_I|}{a}\right) \tag{4.51}$$

and the expression in the spatial coordinate is

$$\Phi_a^X\left(\varphi^{-1}(x,t) - \varphi^{-1}(x_I,t)\right) = \frac{1}{a}\Phi\left(\frac{|x - x_I|}{(1+t)a}\right) \tag{4.52}$$

The material kernel function, plotted in the original and current configurations, is shown in Fig. 2. Note that in this example, Φ is taken as a cubic spline function, the RKPM particles are equally spaced, and the dilation parameter a is selected so that the support of Φ_a^X covers five particles in the undeformed configuration. As can be seen in Fig. 2, Φ_a^X has a fixed support size, $2a$, in the undeformed configuration, and has deformation dependent support size of $2a(1+t)$ when mapped to the current configuration. The support of Φ_a^X covers the same set of particles throughout the deformation with a fixed a and therefore is classified as a "Lagrangian-typed" kernel function. In computational solid mechanics, a material kernel function is more suitable in RKPM computation using a Lagrangian formulation with reference to either the original or current configuration.

4.3.2
Spatial kernel function

One can also define the kernel function in the current configuration as follows:

$$\Phi_a^x(\boldsymbol{x} - \boldsymbol{x}_I) = \frac{1}{a}\Phi\left(\frac{\| \boldsymbol{x} - \boldsymbol{x}_I\|}{a}\right) \tag{4.53}$$

This spatial kernel function can also be expressed in original configuration by the mapping $\boldsymbol{x} = \boldsymbol{\varphi}(\boldsymbol{X}, t)$, i.e.,

$$\Phi_a^x(\boldsymbol{\varphi}(\boldsymbol{X},t) - \boldsymbol{\varphi}(\boldsymbol{X}_I,t)) = \frac{1}{a}\Phi\left(\frac{\|\boldsymbol{\varphi}(\boldsymbol{X},t) - \boldsymbol{\varphi}(\boldsymbol{X}_I,t)\|}{a}\right) \tag{4.54}$$

Equations (4.53) and (4.54) indicate that the spatial kernel function Φ_a^x has fixed support size in current configuration and has deformation dependent support size when expressed in the original configuration. These properties of spatial kernel can be illustrated in the same uniaxial tension problem as defined in Eq. (4.49). The spatial kernel function expressed in the spatial coordinate is

$$\Phi_a^x(x - x_I) = \frac{1}{a}\Phi\left(\frac{|\, x - x_I\,|}{a}\right) \tag{4.55}$$

and the expression of the spatial kernel function using the material coordinate is

$$\Phi_a^x(\varphi(X) - \varphi(X_I)) = \frac{1}{a}\Phi\left(\frac{|\,(1+t)(X - X_I)\,|}{a}\right) \tag{4.56}$$

As presented in Fig. 3, Φ_a^x has fixed support size, $2a$, in the current configuration, and has deformation dependent support size, $2a/(1+t)$, when mapped to the original configuration. The number of particles covered under the support varies with deformation when the dilation parameter is fixed. Since the spatial kernel function has a fixed support size in the current configuration, it is a "Eulerian-typed" kernel function. As can be seen in this uniaxial tension example, the spatial kernel function will encounter numerical instability when $t > 1$ if no re-adjustment in the dilation parameter is performed, whereas the material kernel function avoids this difficulty. Although the spatial kernel function with a fixed dilation parameter is less adequate for structural problems, the function naturally fits the Eulerian formulation in which case the RKPM particles are fixed in space.

4.4
Numerical procedures

In nonlinear problems, incremental and iterative procedures are required. This section outlines the numerical procedures for RKPM hyperelasticity computation. For illustration purposes, we define the following notations:

- Ω_X^I: domain of support of the shape function $\Psi_I^a(\boldsymbol{X})$ associated with particle $\boldsymbol{X}_I$
- S^A: $\{\boldsymbol{X}_I : \boldsymbol{X}_A \in \Omega_X^I\}$ = a set of particles in which the domain of support associated with each particle covers $\boldsymbol{X}_A$.
- NA: number of particles in set S^A

Figure 4 demonstrates an RKPM discretization. In this simple example, $S^A = \{\boldsymbol{X}_I, \boldsymbol{X}_J, \boldsymbol{X}_K\}$ and $NA = 3$.

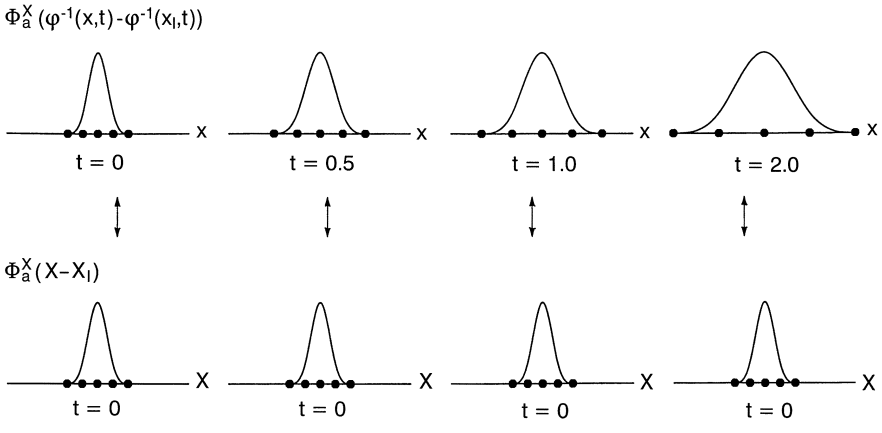

Fig. 2. Material Kernel Function

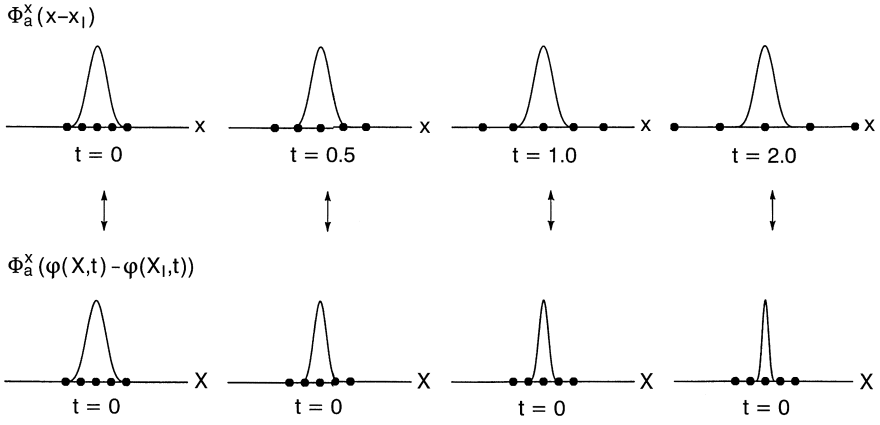

Fig. 3. Spatial Kernel Function

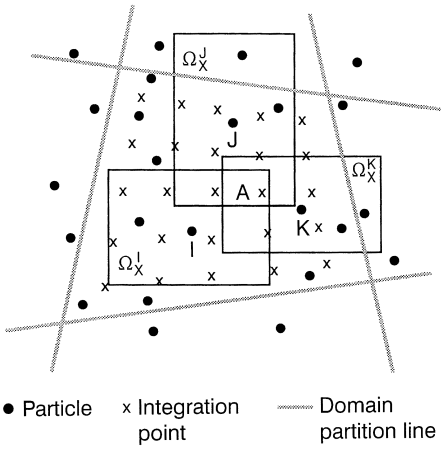

Fig. 4. Graphical Representation of RKPM discretization

In the flow chart of RKPM nonlinear computation for hyperelasticity given below, the transformation method is used to impose essential boundary conditions. Suppose that we are currently at the $(n+1)$-th solution step and $(\nu+1)$-th iteration step (the scripts $n+1$ and $\nu+1$ are dropped for simplicity):

1. Loop over integration zone
   1.1. Loop over integration points $\boldsymbol{X}_A$
      1.1.1. Loop over all particles $\boldsymbol{X}_I \in S^A$
         1.1.1.1. Compute the shape function: $\Psi_I^a(\boldsymbol{X}_A)$
         1.1.1.2. Compute the material derivatives of shape function: $\frac{\partial \Psi_I^a}{\partial X_i}(\boldsymbol{X}_A)$.
      1.1.2. End of particle loop
      1.1.3. Compute deformation gradient:
$$F_{ij}(\boldsymbol{X}_A) = \sum_{I=1}^{NP}\left[\frac{\partial \Psi_I^a}{\partial X_j}(\boldsymbol{X}_A) d_{iI}\right] + \delta_{ij}$$
      1.1.4. Use deformation gradient to compute the following quantities at integration point $\boldsymbol{X}_A$
      Green-Lagrangian strain $E_{ij}(\boldsymbol{X}_A)$, and Green deformation tensor $G_{ij}(\boldsymbol{X}_A)$,
      reduced invariants $\bar{I}_1(\boldsymbol{X}_A), \bar{I}_2(\boldsymbol{X}_A), J(\boldsymbol{X}_A)$
      second Piola-Kirchhoff stress $S_{ij}(\boldsymbol{X}_A)$
      material response matrix $\boldsymbol{C}(\boldsymbol{X}_A)$
      1.1.5. Use second Piola-Kirchhoff stress to compute the following matrices at integration point $\boldsymbol{X}_A$
      stress vector $\boldsymbol{\Xi}(\boldsymbol{X}_A)$
      initial stress matrix $\boldsymbol{T}(\boldsymbol{X}_A)$
      1.1.6. Loop over particles $\boldsymbol{X}_1 \in S^A$
         1.1.6.1. Form gradient matrices $\boldsymbol{B}_I^G(\boldsymbol{X}_A), \boldsymbol{B}_I^M(\boldsymbol{X}_A)$
         1.1.6.2. Form internal force vector $\boldsymbol{f}_I^{int}$ and external force vector $\boldsymbol{f}_I^{ext}$ and assemble residual force $\Delta \boldsymbol{f}_I$
      1.1.7. Loop over particle $\boldsymbol{X}_J \in S^A$
         1.1.7.1. Form gradient matrices $\boldsymbol{B}_J^G(\boldsymbol{X}_A), \boldsymbol{B}_J^M(\boldsymbol{X}_A)$
         1.1.7.2. Form and assemble material and geometric stiffness matrices $\boldsymbol{K}_{IJ}^G, \boldsymbol{K}_{IJ}^M$
      1.1.8. End of particle loop
   1.2. End of integration point loop
2. End of integration zone loop
3. Transform stiffness matrix and force vector and Solve $\hat{\boldsymbol{K}}\Delta\hat{\boldsymbol{d}} = \Delta\hat{\boldsymbol{f}}$
4. Transform $\Delta\hat{\boldsymbol{d}}$ to $\Delta\boldsymbol{d}$, and update displacements
5. If converged, update displacements, $n \leftarrow n+1$ and go to the next solution step; otherwise, $\nu \leftarrow \nu+1$ go to the next iteration.

5
Solution existence in RKPM discretized hyperelasticity

5.1
Overview of the existence conditions in hyperelasticity

The sufficient conditions of the solution existence of a C^0 finite element discretization in nearly incompressible and incompressible hyperelasticity have been discussed by Chen and Han, Wu, and Duan (1995c) based on the existence results proved by Charrier, Dacorogna, Hanouzet, and Laborde (1988). Since in the present approach the RKPM employs Galerkin approximation in conjunction with RKPM shape function of class C^m, we shall reexamine the solution existence conditions of RKPM discretization for hyperelasticity problems based on the existence results proved by Charrier et al. (1988). The following standard notations defined at the undeformed configuration are used for the function spaces,

$$L^q(\Omega_X) = \left\{ v : \int_{\Omega_X} |v(\boldsymbol{X})|^q d\Omega_X < \infty \right\}, 1 \le q \le \infty \ , \tag{5.1}$$

$$L^{\infty}(\Omega_X) = \left\{ v : \text{ess sup}_{X \in \Omega_X} |v(X)| < \infty \right\} \ , \tag{5.2}$$

and for the Sobolev spaces

$$W^{1,q}(\Omega_X) = \left\{ v \in L^q(\Omega_X) : \frac{\partial v}{\partial X_i} \in L^q(\Omega_X), \right\} \ , \quad 1 \le i < 3\}, 1 \le q < \infty, \tag{5.3}$$

$$W^{I,\infty}(\Omega_X) = \left\{ v \in L^{\infty}(\Omega_X) : \frac{\partial v}{\partial X_i} \in L^{\infty}(\Omega_X), \right\} \ , 1 \le i < 3 \ , \tag{5.4}$$

$$W^{l,q}(\Omega_X; R^3) = \left[W^{1,q}(\Omega_X) \right]^3 \tag{5.5}$$

The existence results of the hyperelasticity problem proved by Charrier et al. (1988) are summarized as follows:

Theorem 5.1 Assume the deviatoric strain energy density function $\overline{W}$, the volumetric strain energy function $\tilde{W}$, the external energy U^{ext}, and the material deformation satisfy the following conditions:

(a) The deviatoric strain energy density function $\overline{W}$ is assumed to be expressed in the following form,

$$\overline{W}(\bar{I}_1, \bar{I}_2) = \overline{w}(J^{-1/3}\nabla\boldsymbol{\varphi}, \text{adj}(J^{-1/3}\nabla\boldsymbol{\varphi})) \tag{5.6}$$

where

$$\overline{w}(\boldsymbol{A}, \boldsymbol{B}) = \sum_{i=1}^{M} a_i (\text{tr}(\boldsymbol{A}^T\boldsymbol{A}))^{\alpha_i/2} + \sum_{i=1}^{N} b_i (\text{tr}(\boldsymbol{B}^T\boldsymbol{B}))^{\beta_i/2} + c \tag{5.7}$$

with coefficients $a_i, \alpha_i, b_i, \beta_i$ satisfying the following conditions:

$$a_i > 0, \qquad \alpha_i \ge \frac{3}{2}, \qquad b_i > 0, \qquad \beta_i \ge 3 \tag{5.8}$$

(b)The volumetric strain energy density function $\tilde{W}(J) = kG(J)$ is assumed to satisfy

$$G : (0, +\infty) \to (0, +\infty) \quad \text{is convex;} \tag{5.9}$$

$$\lim_{J \to 0_+} G(J) = +\infty \tag{5.10}$$

$$G(J) \ge cJ^{\gamma} \quad \text{for some } c > 0 \text{ and } \gamma > 1, \text{ when } J \text{ is large enough;} \tag{5.11}$$

$$G(J) = 0 \text{ if and only if } J = 1 \tag{5.12}$$

(c) Let $\alpha = \max\{\alpha_i, 1 \le i \le M\}$ and $\beta = \max\{\beta_i, 1 \le i \le N\}$, then the following conditions are assumed to be satisfied:

$$p \equiv \frac{3\alpha\gamma}{\alpha + 3\gamma} > \frac{3}{2}; \ q \equiv \frac{3\beta\gamma}{2\beta + 3\gamma}; \ \frac{1}{p} + \frac{1}{q} = \frac{1}{\alpha} + \frac{1}{\beta} + \frac{1}{\gamma} < \frac{4}{3} \tag{5.13}$$

(d) The external energy U^{ext} is assumed to be a continuous functional of V where

$$V = \{\boldsymbol{\varphi} \in \boldsymbol{W}^{l,p}(\Omega_X; R^3) : \text{adj } \nabla\varphi \in [L^q(\Omega_X)]^{3\times 3}, \det \nabla\boldsymbol{\varphi} \in L^{\gamma}(\Omega_X), \det \nabla\boldsymbol{\varphi} > 0 \text{ almost everywhere in } \Omega_X, \varphi_i = g_i \text{ on } \Gamma_X^{gi}\} \tag{5.14}$$

(e) There exists a $\boldsymbol{\phi} \in V$ such that the potential energy $U(\boldsymbol{\phi}) < \infty$, where

$$U(\boldsymbol{\phi}) = \int_{\Omega_X} \left[\overline{W}(\bar{I}_1(\boldsymbol{\phi}), \bar{I}_2(\boldsymbol{\phi})) + \tilde{W}(J(\boldsymbol{\phi})) \right] d\Omega - U^{ext} \tag{5.15}$$

If conditions (a)–(e) are satisfied, then there exists a $\boldsymbol{\varphi} \in V$, such that

$$U(\boldsymbol{\varphi}) = \inf\{U(\boldsymbol{\phi}) : \boldsymbol{\phi} \in V\} \tag{5.16}$$

Note that assumptions (5.6) to (5.13) are needed in a mathematical proof of the existence of a solution of the hyperelasticity problem. In practical problems, these assumptions are not always satisfied; for example, a Mooney-Rivlin material. It has been shown by Chen et al. (1995b) that although some material strain energy density functions do not satisfy those conditions, the solution still exists.

The limiting behaviour of the nearly incompressible problem when the parameter $k \to \infty$ (or $\varepsilon = \frac{1}{k} \to 0$) was also discussed by Chen, Han, Wu, and Duan (1995c).

5.2 RKPM discretization in hyperelasticity

In this section, we simply assume that the hyperelasticity problem (5.16) has a solution. Then we consider an RKPM discretization of the minimization problem (5.16). In RKPM, the deformation of material, $\boldsymbol{\varphi}(\boldsymbol{X}, t)$, is interpolated by the shape function $\hat{\Psi}_I^a(\boldsymbol{X})$ of class C^m and we denote this RKPM discretized material deformation by $\varphi^a(\boldsymbol{X}, t)$. An RKPM space $\overline{V}^a$ is defined by

$$\overline{V}^a = \left\{ \boldsymbol{\varphi}^a \in C^m(\Omega_X) : \varphi^a \in \text{span}\{\hat{\Psi}_I^a\}_{I=1}^{NP} \right\} \tag{5.17}$$

Since the shape function $\hat{\Psi}_I^a(\boldsymbol{X})$ possesses Kronecker delta properties, the essential boundary conditions can be represented exactly by functions in $\overline{V}^a$. A set for RKPM approximation is defined as

$$V^a = \left\{ \boldsymbol{\varphi}^a \in \overline{V}^a : \det \nabla\boldsymbol{\varphi}^a > 0 \text{ almost everywhere in } \Omega_X, \varphi_i^a = g_i \text{ on } \Gamma_X^{gi} \right\} \tag{5.18}$$

The RKPM discretization of problem (5.16) is to find $\boldsymbol{\varphi}^a \in V^a$, such that

$$U(\boldsymbol{\varphi}^a) = \inf\{U(\boldsymbol{\phi}^a) : \boldsymbol{\phi}^a \in V^a\} \tag{5.19}$$

The hypotheses (5.6) to (5.13) of Theorem 5.1 are assumed to be satisfied and the functional U^{ext} is continuous on V^a. Since we have

$$\boldsymbol{\varphi}^a \in W^{1,\infty}(\Omega_X; R^3) \ , \tag{5.20}$$

$$\det \nabla\boldsymbol{\varphi}^a \in L^{\infty}(\Omega_X) \ , \tag{5.21}$$

$$\text{adj } \nabla\boldsymbol{\varphi}^a \in [L^{\infty}(\Omega_X)]^{3\times 3} \ . \tag{5.22}$$

Thus, for any $p, q, \gamma \in [1, \infty)$ and in particular for p, q, γ satisfying Eq. (5.13), we have

$$\boldsymbol{\varphi}^a \in W^{1,p}(\Omega_X; R^3) \ , \tag{5.23}$$

$$\det \nabla\boldsymbol{\varphi}^a \in L^{\gamma}(\Omega_X) \ , \tag{5.24}$$

$$\text{adj } \nabla\boldsymbol{\varphi}^a \in [L^{q}(\Omega_X)]^{3\times 3} \ . \tag{5.25}$$

Also for $\boldsymbol{\varphi}^a \in V^a, U(\boldsymbol{\varphi}^a) < \infty$. Under conditions (5.23) to (5.25), the proof by Chen and Han et al. (1995c) can be adapted to show that problem (5.19) has a solution.

Note that if $\Psi_I^a(\boldsymbol{X})$ is used as the RKPM shape function and a Lagrangian multiplier method is employed to enforce the essential boundary conditions, then the minimization problem becomes a saddle problem and the existence conditions discussed in this section are not applicable.

6
Numerical Examples

The strain energy density function given in Eqs. (2.8)–(2.10) is employed in the following study. Unless specified, the material properties A_{10} = 0.373 MPa, A_{20} = −0.031 MPa, A_{30} = 0.005 MPa, $k = 10^5$ MPa taken from Chen et al. (1995b) are used in the numerical examples. The Cubic spline with a correction function constructed by satisfying linear reproducing conditions is used as the modified kernel function, and a normalized dilation parameter is defined by

$$r_i = \frac{a_i}{2d_i^{\max}} \tag{6.1}$$

where r_i and $d_i^{\max}$ are the normalized dilation parameter and the maximum particle distance in i-th direction, respectively. Unless specified otherwise, Gauss quadrature of $(\sqrt{n}+2) \times (\sqrt{n}+2)$, with n the total number of particles in the integration zone is used for RKPM domain integration.

6.1
Uniaxial tension-compression of a plane-strain rubber unit

A 1.0 cm × 0.25 cm plane-strain rubber unit is subjected to tension and compression along the axial direction. To generate uniaxial deformation, no constraints are imposed in the lateral direction on the two ends. In this problem, the displacement field in the structure at any instant of time is linear, and the nonlinear stress-strain behavior is due to material nonlinearity. Therefore, RKPM with a modified kernel function that satisfies reproducing conditions in a linear field is expected to provide a very accurate solution for this problem.

To study the effect of particle irregularity on the solution accuracy, two particle models as shown in Fig. 5 are used in the analysis. A total of 4×1 equal-sized integration zones are used to perform numerical integration. The specimen is stretched to 10 times of its original axial length in tension, and is compressed until the deformed axial length reaches 1/10 of its original size. In Fig. 5, the reduced stress is defined by $t/(\lambda^2 - \lambda^{-2})$ with t the axial Cauchy stress and λ the axial stretch ratio.

Both regularly spaced and irregularly spaced particle models, with various dilatation parameters, $r_i = 0.5, 0.75, 1.0$, are used in the analysis. The predicted reduced stress versus stretch ratio are compared against the incompressible solution in Fig. 5. Since material kernel functions are used in the analysis, there is no need to readjust dilatation parameter during deformation. In this example, the dilation parameter, particle density, and particle distribution have no effect on the results. This is expected, because the employed modified kernel function satisfies reproducing conditions in the linear field. The progressive deformations of the irregularly spaced particle model are plotted in Fig. 6. The numerical errors in this problem are due to the finite bulk modulus being used in the analysis.

6.2
Simple shear test

A test specimen of 0.25 cm × 1.0 cm is subjected to a simple shear deformation. According to the laboratory simple shear test fixture, the thickness of the specimen remains constant while sheared. The same particle models as used in example 6.1 are used for this analysis. Similarly, 4×1 integration zones are employed to perform numerical integration.

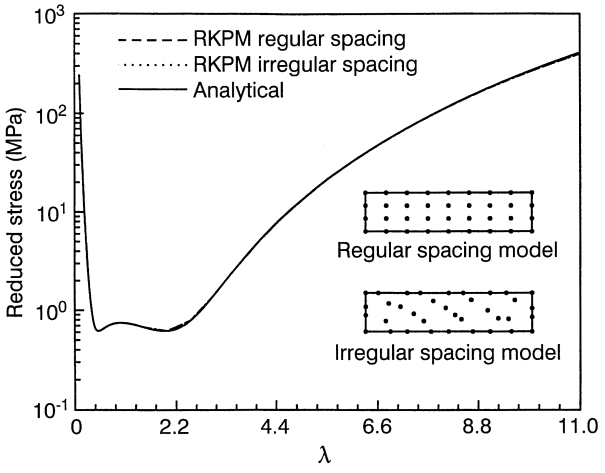

Fig. 5. Rubber under uniaxial tension-compression

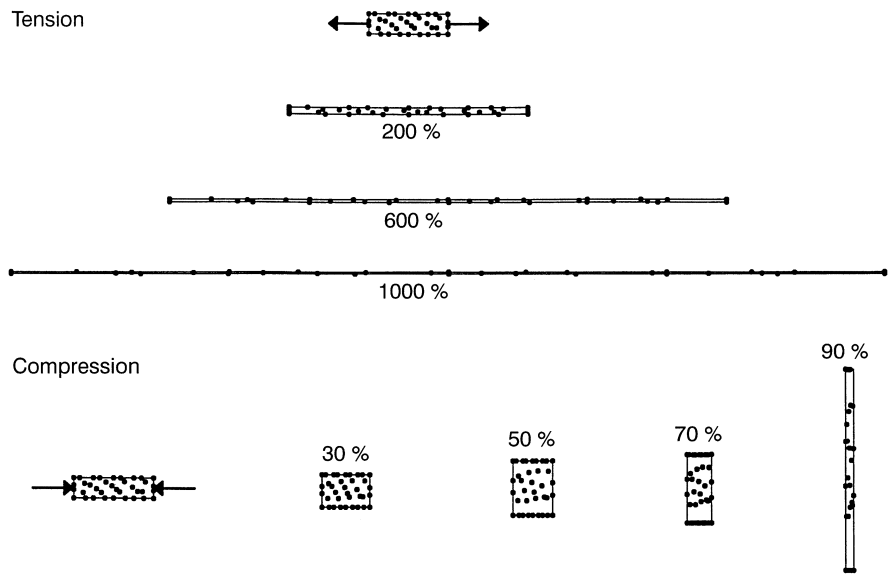

Fig. 6. Deformation of rubber under uniaxial tension and compression

The test specimen is sheared to an engineering shear strain of 200%. Since material kernel functions are employed in the formulation, the dilation parameters are kept constant throughout the course of deformation. The analysis results, obtained from the two discrete particle models with various normalized dilation parameters of $r_i = 0.5, 1.0, 2.0$ are compared with the simple shear solution and experimental data in Fig. 7. A very good agreement is observed between the numerical solution, simple shear solution [Rivlin (1940)], and experimental data [Yeoh (1990)]. Similar to the uniaxial tension-compression problem, the magnitude of normalized dilation parameter does not affect the analysis results in this problem.

6.3
Inflation of an infinitely long rubber tube

This problem exhibits a nonlinear displacement field and nonlinear load-displacement response. An infinitely long tube, with inner radius of 6 cm and outer radius of 8 cm, is analyzed by an axisymmetric RKPM formulation with constraints introduced in the axial direction to impose plane-strain condition as shown in Fig. 8 (a). A total of nine particles are used to discretize the thickness of the tube. Three sets of regularly and irregularly spaced particles as shown in Fig. 8 (a) are used to model the tube. Four equally-spaced integration zones are used in radial direction for numerical integration.

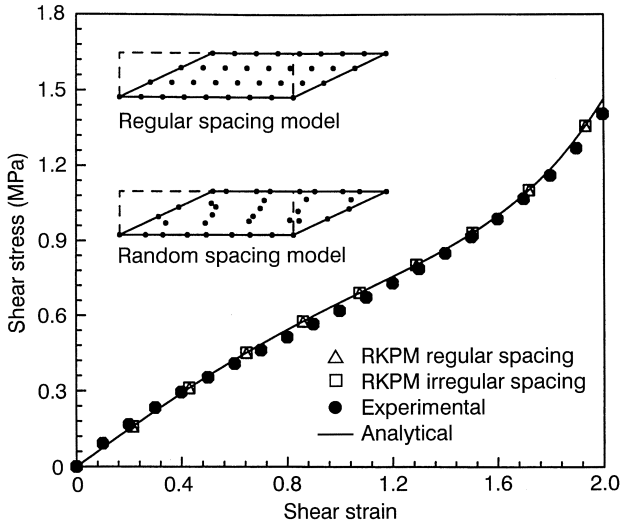

Fig. 7. Rubber shear test

The pressure-displacement curves calculated by the three particle models are compared against the analytical solution [Chen et al. (1995b)] in Fig. 8 (a). The irregularly spaced model (c) generates a somewhat stiffer solution. The effect of the dilatation parameter on the RKPM solution is studied in Fig. 8 (b). In this study, regularly spaced particles are used to model the problem. As can be seen in Fig. 8 (b), when a small dilation parameter is used, the structure behaves stiffly. An accurate solution can be obtained by the use of a larger dilation parameter in the radial direction.

The effect of the dilation parameter on the solution accuracy is also studied by calculating the relative energy error in the following form,

$$e^E = \frac{U^{RKPM}(\boldsymbol{u}^a(p)) - U^{exa}(\boldsymbol{u}(p))}{U^{exa}(\boldsymbol{u}(p))} \tag{6.3}$$

where U^{RKPM} is the internal stored energy calculated using the RKPM solution $\boldsymbol{u}^a$,

$$U(\boldsymbol{u}^a)^{RKPM} = \int_{\Omega_X} W(\bar{I}_1(\boldsymbol{u}^a), \bar{I}_2(\boldsymbol{u}^a), J(\boldsymbol{u}^a))\mathrm{d}\Omega$$

and U^{exa} is the internal stored energy calculated using analytical solution. The relative energy error of the regularly spaced particle model calculated at an internal pressure of 0.46 MPa is shown in Fig. 8 (c). The results indicated that the smaller normalized dilation parameter leads to a higher energy error. As the normalized dilation parameter increases, the energy error generally decreases. The relative energy error is less than 0.2% when $r \geq 1.6$.

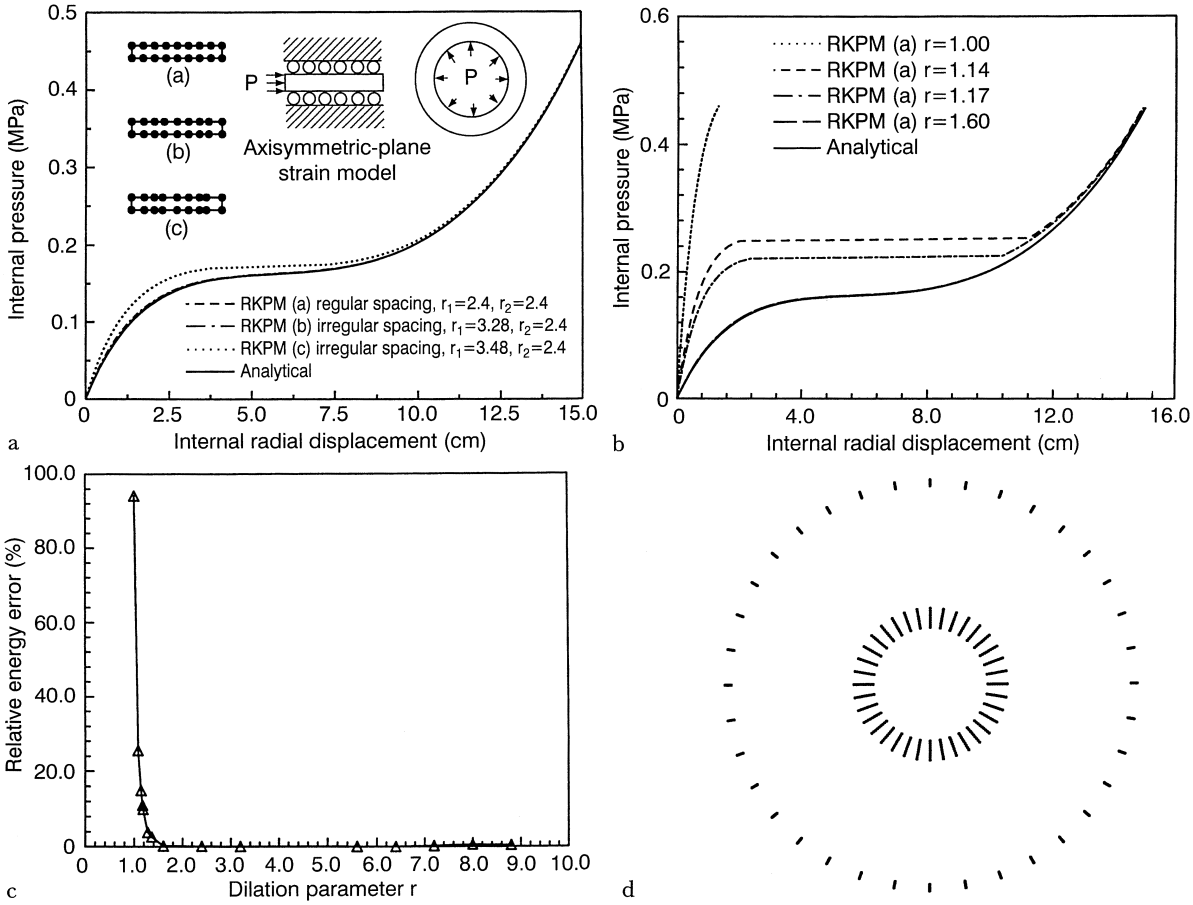

Fig. 8a–d. Inflation of rubber tube: **(a)** Effect of particle spacing **(b)** Effect of dilation parameter **(c)** Relative energy error vs. dilation parameter at pressure = 0.46 MPa **(d)** Undeformed and deformed geometries

The 360 degree undeformed and deformed structures generated by sweeping one particle line in the circumferential direction are plotted in Fig. 8 (d).

6.4 Disk inflation problem

A disk inflation problem is analyzed to examine the ability of RKPM to handle large rotation and large strain. A disk with a radius of 7.45 in (18.923 cm) and thickness of 0.25 in (0.635 cm) is subjected to a uniform pressure load. The material properties obtained from Chang et al. (1991) are A_{10} = 80 psi (0.5516 MPa), A_{01} = 20 psi (0.1379 MPa), and $k = 10^5$ psi (689.5 MPa). The edge of the disk is simply supported. This problem is analyzed by finite element and RKPM for comparison. Three 4-node finite element meshes, each with 10×1 elements (22 nodes), 10×2 elements (33 nodes), and 100×3 elements (404 nodes) are used for finite element analysis. In this finite element formulation, pressure is projected onto a constant field to avoid locking. A 22-node particle model generated using the coarse finite element model is used for RKPM computation. A total of 10×1 integration zones are used for the RKPM domain integration.

A maximum pressure of 0.207 MPa is applied with 207 incremental steps. The analysis results are compared in Fig. 9. The finite element response is stiff when the coarse mesh with only one layer of elements in the thickness of the disk is used. The refined 10×2 finite element mesh generates softer results, yet diverged at an earlier stage. The reproducing kernel particle method, on the other hand, is able to provide results similar to the very refined finite element solution (404 nodes), with far fewer degrees

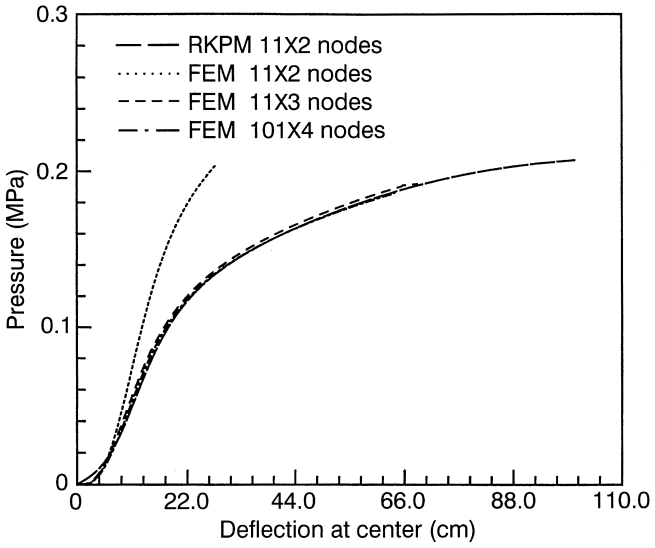

Fig. 9. Inflation of rubber disk: comparison of RKPM and FEM solution

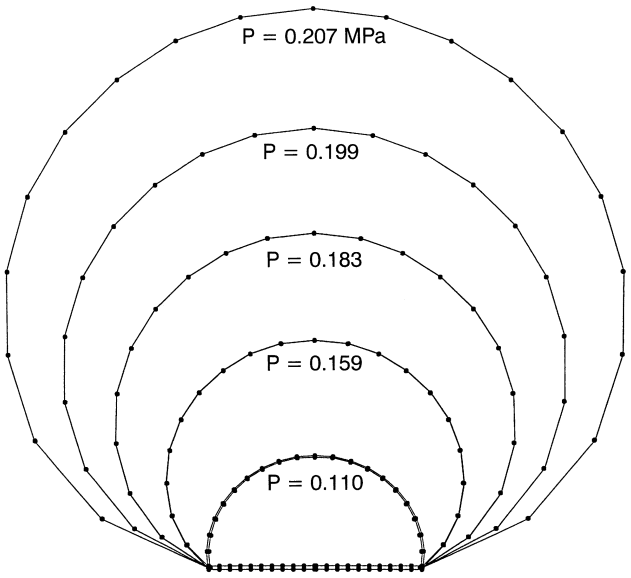

Fig. 10. Inflation of rubber disk: progressive deformations

of freedom (22 nodes). The RKPM deformed shapes are plotted in Fig. 10.

6.5
Analysis of a silentbloc rubber bushing assembly

A typical rubber bushing contains a rubber insert and two concentric metal sleeves. A Silentbloc bushing is assembled by shooting the rubber insert between two lubricated metal sleeves. This problem analyzes rubber deformation induced by the assembly process. The geometries as shown in Fig. 11. and the neo-Hookean material property of $A_{10} = 2.298$ MPa are obtained from Tseng, Satyamurthy, and Chang (1987). The inner and outer radii of metal sleeves are 1.93 cm and 4.37 cm, respectively. The bulk modulus is taken to be $k = 10^3$ MPa.

Since the metal sleeves are much stiffer than the rubber insert, only the rubber insert is modeled, and the metal sleeves are treated as frictionless rigid surfaces. The problem is analyzed by RKPM with normalized dilation parameters of $r_i = 0.8, 0.9, 1.0$ and finite elements (as shown in Fig. 11) for solution comparison. The analysis is performed by 50 incremental steps, and only half of the axisymmetric structure is modeled due to symmetry. In this problem, an analytical solution is not available, and therefore the finite element solution obtained from the 725-node mesh is considered as the benchmark for comparison.

Since in bushing design the axial dimension on the outer radius of the assembled bushing determines the amount of space required for installation, we compare the deformed axial displacements on the outer radius in Table 1. The 56-node RKPM solution is able to approach the much refined

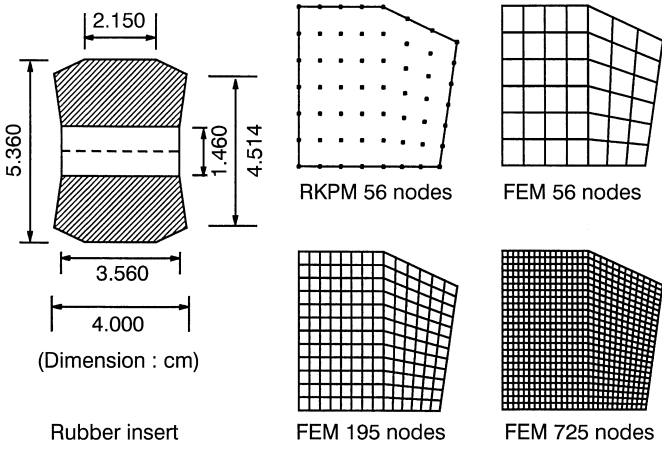

Fig. 11. Analysis of Silentbloc bushing assembly: problem description

725-node finite element solution as the normalized dilation parameter approaches 1.0. The deformed geometries of the assembled bushing are plotted in Fig. 12.

7
Conclusion

A Reproducing Kernel Particle Method for the nonlinear analysis of rubber is presented. This paper proposed several approaches essential to nonlinear hyperelasticity analysis. The major achievements in this work are:

(1) By the use of a material kernel function, the continuous re-adjustment of the dilation parameter in large deformation problems is not required.
(2) A modified RKPM shape function is constructed to allow the direct prescription of essential boundary conditions. The Lagrange multiplier method for hyperelasticity is also discussed.

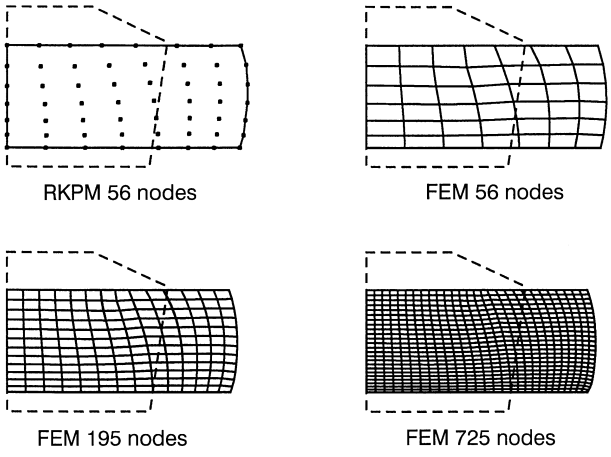

Fig. 12. Analysis of Silentbloc bushing assembly: deformed geometries

Table 1. Comparison of axial displacements on the outer radius of assembled bushing

FEM 56 nodes (42 elements)	FEM 195 nodes (168 elements)	FEM 725 nodes (672 elements)	RKPM 56 nodes $r_1 = r_2 = 0.8$	RKPM 56 nodes $r_1 = r_2 = 0.9$	RKPM 56 nodes $r_1 = r_2 = 1.0$
2.316 cm	2.284 cm	2.256 cm	2.224 cm	2.236 cm	2.256 cm

(3) The solution existence conditions in RKPM discretized hyperelasticity problems are discussed.
(4) The results show absence of volumetric locking in RKPM large deformation analysis of nearly incompressible hyperelasticity. Similar observation was also reported in Belytschko, Lu, and Gu (1994a) using EFG for linear problems.
(5) For the same level of accuracy, RKPM requires far fewer degrees of freedom compared to FEM.

In this study, the effectiveness of RKPM is examined by solving a set of incompressible hyperelasticity problems such as tension, compression, shear, and inflation. The application to engineering elastomers is demonstrated in the analysis of rubber bushing. The numerical examples indicate that the selection of the dilation parameter is critical to solution accuracy. The relationship between the RKPM energy error and dilation parameter is characterized in the inflation problem. The advantages of RKPM over FEM become more clear when dealing with extremely large deformations. Although in this study RKPM demonstrates a promising potential for large deformation problems, a more systematic approach on the appropriate selection of the dilation parameter needs to be made for the method to be more robust.

Appendix

Explicit expressions of material response tensor

The explicit expressions of the material response tensor for nearly incompressible material with the strain energy density function given in Eqs. (2.9)–(2.10) are

$$\begin{aligned}
\overline{C}_{ijkl} &= \frac{\partial^2 \overline{W}}{\partial E_{ij}\partial E_{kl}} \\
&= \frac{2}{3}\overline{K}_1 I_3^{-1/3}\left\{-2\left(\delta_{ij}G_{kl}^{-1}+\delta_{kl}G_{ij}^{-1}\right)\right. \\
&\quad \left.+\frac{1}{3}I_1\left[2G_{ij}^{-1}G_{kl}^{-1}+3\left(G_{ik}^{-1}G_{jl}^{-1}+G_{il}^{-1}G_{jk}^{-1}\right)\right]\right\} \\
&\quad +\frac{4}{3}\overline{K}_2 I_3^{-2/3}\left\{-2I_1\left(\delta_{ij}G_{kl}^{-1}+\delta_{kl}G_{ij}^{-1}\right)\right. \\
&\quad +2\left(G_{ik}^{-1}G_{jl}^{-1}+G_{il}^{-1}G_{jk}^{-1}\right) \\
&\quad \left.+I_2\left(\frac{4}{3}G_{ij}^{-1}G_{kl}^{-1}+G_{ik}^{-1}G_{jl}^{-1}+G_{il}^{-1}G_{kj}^{-1}\right)\right. \\
&\quad \left.+\frac{3}{2}\left[2\delta_{ij}\delta_{kl}-\left(\delta_{ik}\delta_{jl}+\delta_{il}\delta_{kj}\right)\right]\right\} \\
&\quad +4\overline{H}_{11}I_3^{-2/3}\left(\delta_{ij}-\frac{1}{3}I_1G_{ij}^{-1}\right)\left(\delta_{kl}-\frac{1}{3}I_1G_{kl}^{-1}\right) \\
&\quad +4\overline{H}_{12}I_3^{-1}\left[\left(\delta_{ij}-\frac{1}{3}I_1G_{ij}^{-1}\right)\left(I_1\delta_{kl}-G_{kl}\right.\right. \\
&\quad \left.\left.-\frac{2}{3}I_2G_{kl}^{-1}\right)\right]+4\overline{H}_{22}I_3^{-4/3}\left(I_1\delta_{ij}-G_{ij}-\frac{2}{3}I_2G_{ij}^{-1}\right) \\
&\quad \times\left(I_1\delta_{kl}-G_{kl}-\frac{2}{3}I_2G_{kl}^{-1}\right)\ , \qquad (A.1)
\end{aligned}$$

$$\begin{aligned}
\tilde{C}_{ijkl} &= \frac{\partial \tilde{W}}{\partial E_{ij}\partial E_{kl}} = kJ(J-1) \\
&\quad \times\left(G_{ij}^{-1}G_{kl}^{-1}-G_{ik}^{-1}G_{jl}^{-1}-G_{il}^{-1}G_{jk}^{-1}\right)+kJ^2G_{ij}^{-1}G_{kl}^{-1} \qquad (A.2)
\end{aligned}$$

where

$$\overline{H}_{ij} = \frac{\partial^2 W}{\partial \overline{I}_i \partial \overline{I}_j} \qquad (A.3)$$

References

Bercovier, M. (1978): Perturbation of mixed variational problems, application to mixed finite element methods. R. A. I. R. O. Num. Anal. 12: 211–236

Belytschko, T.; Lu Y. Y.; Gu, L. (1994a): Element-free Galerkin methods Int. J. Numer. Meth. Eng. 37: 229–256

Belytschko, T. (1994b): Are finite elements passé ? USACM Bulletin 7: 4–7

Belytschko, T.; Gu, L.; Lu, Y. Y. (1994c): Fracture and crack growth by EFG method, Modeling Simul. Mater. Sci. Eng., 2: 519–534

Belytsehko, T.; Organ, D.; Krongarz, Y. (1995): A coupled finite element–element-free Galerkin method, Comput. Mech. 177: 186–195

Chang, T. Y. P.; Saleeb, A.-F.; Li, G. (1991): Large strain analysis of rubber-like materials based on a perturbed lagrangian variational Principle. Comput. Mech. 8: 221–233

Charrier, P.; Dacorogna, B.; Hanouzet, B.; Laborde, P. (1988): An existence theorem for slightly compressible materials in nonlinear elasticity. SIAM, J. Math. Anly. 19: 70–85

Chen, J.-S.; Satyamurthy, K.-S.; Hirschfelt, L.-R. (1994): Consistent finite element procedures for nonlinear rubber elasticity with a higher order strain energy function. Comput. & Struct. 50: 715–727

Chen, J.-S.; Pan, C. (1995a): A pressure projection method for nearly incompressible rubber hyperelasticity, Part I: Theory, in press, Journal of Applied Mechanics

Chen, J.-S.; Wu, C.-T.; Pan, C. (1995b): A pressure projection method for nearly incompressible rubber hyperelasticity, Part II: applications, in press, Journal of Applied Mechanics

Chen, J.-S.; Han, W.; Wu, C.-T.; Duan, W. (1995c): On the perturbed Lagrange formulation for nearly incompressible and incompressible hyperelasticity, in press, Comput. Meth. Appl. Mech. Engng

Chen, J.-S.; Pan, C.; Chang, T.-Y.-P. (1995d): On the control of pressure oscillation in bilinear-displacement constant-pressure element. 128: 137–152

Gent, A.-N.; Lindley, P.-B. (1959): The compression of bonded rubber blocks. Proc. Inst. Mech. Engrs. 173: 111–122

Herrmann, L.-R. (1965): Elasticity equations for incompressible and nearly incompressible materials by a variational theorem. AIAA Jnl. 3: 1896–1900

Johnson, G.-R.; Peterson, E.-H.; Stryrk, R.-A. (1993): Incorporation of an SPH option into the EPIC code for a wide range of high velocity impact computations, preprint

Key, S.-W. (1969): A variational principle for incompressible and nearly incompressible anisotropic elasticity. Int. J. Solids Struct. 5: 951–964

Libersky, L.-D.; Petschek, A.-G.; Carney, T.-C.; Hipp, J.-R.; Allahdadi, F.A. (1993): High strain Lagrangian hydrodynamics. J. Comp. Phys. 109: 67–75

Liu, W.-K.; Ong, J.-S.-J.; Uras, R.-A. (1985): Finite element stabilization matrices – A unification approach. Comput. Meth. Appl. Mech. Engng. 53: 13–46

Liu, W.-K.; Belytschko, T.; Chen, J.-S. (1988): Nonlinear versions of flexurally superconvergent elements. Comput. Meth. Appl. Mech. Engng. 71: 241–256

Liu, W.-K.; Jun, S.; Li, S.; Adee, J.; Belytschko, B. (1995a): Reproducing kernel particle methods for structural dynamics. Int. J. Numer. Meth. Eng. 38: 1655–1679

Liu, W.-K.; Jun, S.; Zhang, Y.-F. (1995b): Reproducing kernel particle methods. Int J. Numer. Meth. Fluids. 20: 1081–1106
Liu, W.-K. (1995c): An introduction to wavelet reproducing kernel particle methods. USACM Bulletin. 8: 3–16
Liu, W.-K.; Chen, Y. (1995d): Wavelet and multi-scale reproducing kernel particle methods. Int. J. Numer. Meth. Fluids. 21: 901–931
Liu, W.-K.; Li, S.; Belytschko, T. (1995e): Moving least square kernel Galerkin method (I) methodology and convergence, to appear, Comput, Meth. Appl. Mech. Engng
Liu, W.-K.; Chen, Y.; Jun, S.; Chen, J.-S.; Belytschko, T.; Pan, C.; Uras, R.-A.; Chang, C.-T. (1996a): Overview and applications of the reproducing kernel particle methods. Archives of Computational Methods in Engineering State of Art Reviews. 3: 3–80
Liu, W.-K.; Chen, Y.; Chang, R.-A.; Chang C.-T. (1996b): Generalized multiple scale reproducing kernel particle methods, to appear, Comput. Meth. Appl. Mech. Engng.
Lu, Y.-Y.; Belytschko, T.; Gu, L. (1994): A new implementation of the element free Galerkin method. Comput. Meth. Appl. Mech. Engng. 113: 397–414
Malkas, D.-S.; Hughes, T.-J.-R. (1978): Mixed finite element methods-reduced and selective integration techniques: a unification of concept. Comput. Meth. Appl. Mech. Engng. 15: 63–81
Monaghan, J.-J. (1982): Why particle methods work. SIAM J. Sci. Stat. Comput. 3: 422–433
Monaghan, J.-J. (1988): An introduction to SPH. Computer Physics Communications, 48. 89–96
Mooney, M (1940): A theory of large elastic deformation. J. Appl. Phys. 11: 582–592
Penn, R.-W. (1970): Volume changes accompanying the extension of rubber. Trans. Soc. Rheo. 14: 4, 509–517
Rivlin, R.-S. (1956): Rheology theory and applications, ed. F. R. Eirich, 1, Chap. 10, 351–385, Academic Press, New York, NY
Tong, P. (1969): An assumed stress hybrid finite element method for an incompressible and nearly-incompressible material Int. J. Solids Struct. 5: 455–461
Tseng, N.-T.; Satyamurthy, K.; Chang, J.-P. (1987), Nonlinear finite element analysis of rubber based products, Rubber Division, Montreal, Quebec, May 26–29
Yeoh, O.-H. (1990): Characterization of elastic properties of carbon black filled rubber vulcanizates. Rubb. Chem. Technol. 63: 792–805
Yeoh, O.-H. (1993): Some forms of the strain energy function for rubber. Rubb. Chem. Technol. 66: 754–771